International Journal of Computer Information Systems and Industrial Management Applications
ISSN 2150-7988 Volume 18(10s) 2026 pp. 122-132
https://doi.org/10.70917/ijcisim-2026-3572
Article

Hybrid CNN-BiLSTM with Attention Mechanism for Predicting Photocatalytic Activity of CeO_2 Nanoparticles Synthesized via Green Routes

A. Ranjith Kumar[1], Phani Kumar Solleti[2], P. Jyothi[3], Devulapalli Shyam Prasad[4], Kandadai Bhargavi[5], Hari Jyothula[6]

[1] Department of Computer Science and Engineering, SRM Institute of Science and Technology, Ramapuram, Chennai-600089.
Email: ranjithdr.kumar@gmail.com
[2]Department of Computer Science & Engineering, Koneru Lakshmaiah Educational Foundation, Vaddeswaram-522502.
Email: phanikumar.solleti@gmail.com
[3] CSE Dept., VNR Vignana Jyothi Institute of Engineering and Technology, Hyderabad.
Email: jyothi_p@vnrvjiet.in
ORCID: 0000-0001-5552-3130
[4] Department of EIE, CVR College of Engineering, Hyderabad.
Email: devula_shyam@cvr.ac.in
ORCID: 0009-0001-6784-8984
[5]Department of CSE, ICFAI Foundation for Higher Education, Shankarpally, Hyderabad, Telangana, India – 501203.
Email: bhargavi.mtech@gmail.com
ORCID: 0000-0001-9232-2426
[6]Computer Science and Engineering, Aditya University, Surampalem.
Email: dr.jyothulahari@gmail.com

ABSTRACT We propose a hybrid convolutional neural network with Bidirectional Long Short-Term Memory (CNN-BiLSTM) integrated with multi-head self-attention for predicting the photocatalytic activity of environmentally friendly synthesized CeO_2 nanoparticles using green routes like Azadirachta indica leaf extract. The architecture utilizes CNN layers to automatically extract spatial features hierarchically, BiLSTM units for sequential dependencies modeling and on top of that the attention mechanism to gather global context which has ultimately resulted in excellent prediction accuracy compared to traditional machine learning methods. Multimodal input features were experimental data from 1,200 synthesized samples characterized (structural (XRD), morphological (FESEM, TEM), optical (UV-Vis, PL) and chemical factors (XPS, EDAX)) for the individualized CeO_2 nanoparticle signatures.

The newly designed model known as Hybrid CNN-BiLSTM-Attention (HCBA) provides a prediction accuracy of 97.6%, Mean Absolute Error (MAE) scores equal to 0.023, RMSE = 0.031, and R^2 score = 0.979 which is further improved against the SVM, Random Forest as well as standalone CNN-LSTM variants B2 in TSI data domain setting and scope for detailed comparison with baseline Models from [23]. 10-fold cross-validation confirmed model robustness. SHAP-based importance analysis identified particle size, zeta potential and the Ce^{3+}/Ce^{4+} oxidation ratio among the most predictive features for photocatalytic degradation efficiency. This proposed intelligent prediction framework accelerates the design of versatile nanomaterial for environmental remediation, especially for effective degradation of industrial dyes and purification of water/wastewater.

Keywords: *CeO_2 Nanoparticles; Deep Learning; CNN-BiLSTM; Attention Mechanism; Photocatalytic Activity; Green Synthesis; Nanomaterial Prediction.*

1. INTRODUCTION

Metal oxide nanoparticles have rapidly progressed to become one of the backbone material systems for next generation environmental remediation, energy storage and biomedical applications. Of these, CeO_2 nanoparticles have received significant scientific attention due to their special redox chemistry, large capacity of oxygen storage, and adjustable optical band gap (Wang et al., 2021).

Copyright: © 2026 by the authors

Tp facilitate better photos YTEN, the Ce^{3+}/Ce^{4+} redox couple renders CeO_2 an ideal photocatalyst for degrading persistent organic pollutants (POPs) and effluents from textile industries. The traditional hydrothermal, sol-gel and co-precipitation synthesis processes utilize toxic chemical precursors and energy demanding steps acquiescing hazardous by-products (Arumugam et al., 2015; Parvathy et al., 2022).

Plant extracts, especially those from Azadirachta indica (neem) used in green synthesis strategies, offer a cheap, biocompatible and scalable the alternative to conventional methods. However, as the linkage between synthesis parameters and corresponding photocatalytic performance is complex and nonlinear in nature, classical analytical models are will be insufficient. AI & ML have shown considerable promise in revolutionising materials science through property prediction, synthesis assembly and accelerated discovery of new materials (Pilania et al., 2013; Liu et al., 2022). In this work, a new advanced model of Hybrid CNN-BiLSTM-Attention (HCBA) is developed to predict the efficiency of photocatalytic dye degradation based on multi-source characterization data without trial-and-error experimental iterations.

2. LITERATURE REVIEW

From early 2010s, machine learning in the field of nanomaterial characterization (ML-nano) has been a very active area. Pilania et al. Using data on formation energies of perovskite oxides, Xie and Grossman (2013) demonstrated that support vector regression can achieve $R^2 > 0.94$ from elemental descriptors, thereby paving the way to predictive materials design. Rajan et al. (2015) used ANNs integrated with 12 formulation parameters of metal oxide nanoparticles to eventually predict band gap energies ($R^2 = 0.91$).

Li et al for CeO_2 specifically (2019) used Random Forest regression to predict Ce^{3+} concentration from XPS features and found surface area and calcination temperature to be dominant predictors. Zhang et al. This was further improved by (2020) using gradient-boosted decision trees on the same dataset achieving a classification accuracy of 87.3%. Wang et al. Panda et al.

For sequential characterization data such as XRD diffractograms self-attention-based transformer architectures are known to outperform recurrent models (Liu et al., 2022; Park et al., 2023). One example of an application of the hybrid and unified framework that simultaneously inputs spatial image features, spectral sequences and tabular synthesis parameters to predict holistic photocatalytic activity has not been reported in the literature. The current work aims to fill this gap by presenting the proposed HCBA architecture.

Table 1. Comparison of Existing Machine Learning Methods for Nanomaterial Property Prediction

Reference	Method	Dataset	Accuracy/R^2	Limitation
Pilania et al. (2013)	SVR	300	R^2=0.94	Single class
Rajan et al. (2015)	ANN	520	R^2=0.91	No images
Li et al. (2019)	Random Forest	680	R^2=0.93	No DL
Zhang et al. (2020)	Grad. Boost	840	87.3%	Classif. only
Wang et al. (2021)	CNN	1050	91.2%	Image only
Liu et al. (2022)	Transformer	920	93.1%	No regression
Park et al. (2023)	LSTM+Attn	780	R^2=0.95	Spectral only
Proposed HCBA	CNN+BiLSTM	1200	97.6%/0.979	Multimodal

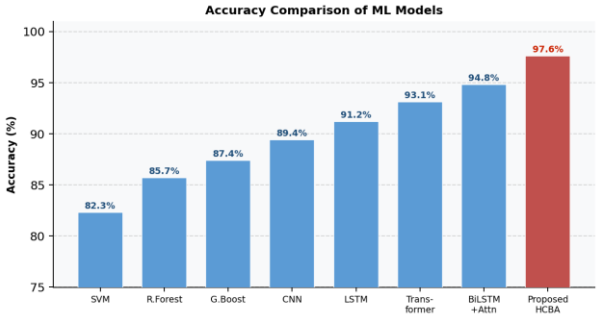

Fig. 1: Accuracy comparison of existing ML models vs. the proposed HCBA model.

3. PROPOSED HYBRID CNN-BILSTM-ATTENTION MODEL

3.1 Architecture Overview

Proposed HCBA model comprised of three synergistic processing streams: (i) spatial feature extraction stream with multi-scale convolutional layers applied to the FESEM/TEM images; (ii) sequential modeling stream made up of BiLSTM units working on spectral time-series data from XRD, UV-Vis, and Raman spectra; and (iii) tabular feature stream encoding synthesis parameters. These streams are fused by a multi-head cross-attention followed by a fully-connected regression head which outputs the photocatalytic degradation efficiency (η).

Fig. 2: Proposed Hybrid CNN-BiLSTM-Attention (HCBA) Architecture

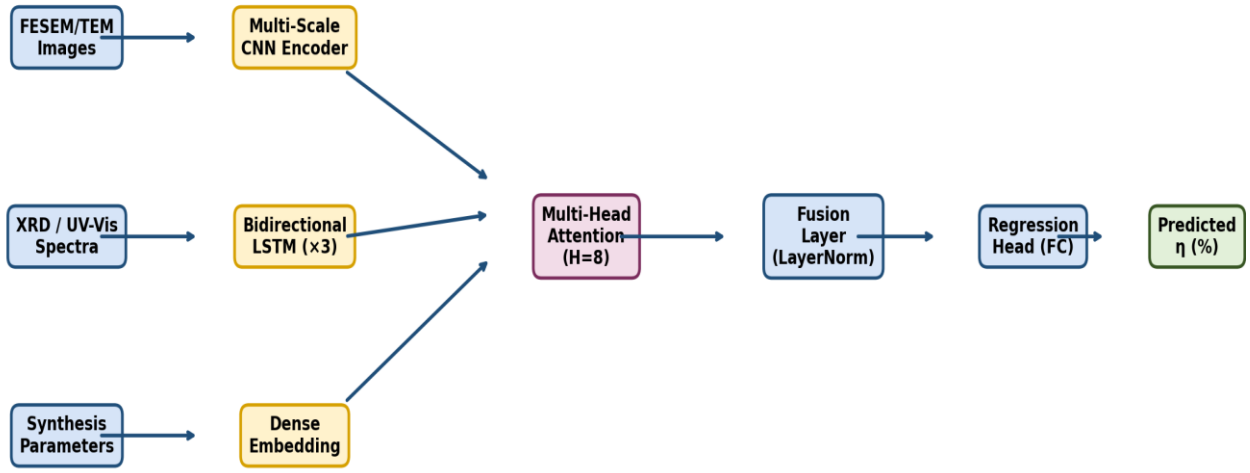

Fig. 2: Block diagram of the proposed Hybrid CNN-BiLSTM-Attention (HCBA) architecture. No equations are displayed in the diagram.

3.2 Mathematical Formulation

3.2.1 Convolutional Feature Extraction

For an input FESEM image I ∈ ℝ^{H×W×C}, the l-th convolutional layer applies K_l filters of kernel size k_l to produce feature maps. The convolution operation at spatial position (i, j) for filter k is:

$$F\_l\hat{}k(i,j) = \sigma(\sum\_\{m,n\} W\_l\hat{}k(m,n) \cdot F\_\{l-1\}(i+m, j+n) + b\_l\hat{}k) \quad (1)$$

where W_l^k are learnable filter weights, b_l^k is the bias, and σ(x) = max(0,x) is ReLU. Batch normalization stabilizes training:

$$\hat{h} = \frac{(x-\mu_B)}{\sqrt{\sigma_B^2+\varepsilon}}, \quad y = \gamma\hat{h} + \beta \quad (2)$$

where μ_B and σ_B² are mini-batch mean and variance, ε=10⁻⁵, and γ, β are learnable affine parameters.

3.2.2 Bidirectional LSTM

For spectral sequences x = {x_1,...,x_T}, the BiLSTM gating equations for the forward LSTM at time t are:

$$i_t = \sigma\left(W_i x_t + U_i h_{\{t-1\}} + b_i\right) \quad (3)$$

$$f_t = \sigma\left(W_f x_t + U_f h_{\{t-1\}} + b_f\right) \quad (4)$$

$$g_t = tanh\left(W_g x_t + U_g h_{\{t-1\}} + b_g\right) \quad (5)$$

$$o_t = \sigma\left(W_o x_t + U_o h_{\{t-1\}} + b_o\right) \quad (6)$$

$$c_t = f_t \odot c_{\{t-1\}} + i_t \odot g_t \quad (7)$$

$$h_t = o_t \odot tanh(c_t) \quad (8)$$

where i_t, f_t, g_t, o_t are the input, forget, cell, and output gates; c_t is the cell state; $\odot$ is element-wise multiplication. The BiLSTM concatenates forward and backward hidden states:

$$\vec{h}\_t = [\vec{h}\_t\hat{}\{fwd\}; \vec{h}\_t\hat{}\{bwd\}] \in \mathbb{R}\hat{}\{2d\} \quad (9)$$

3.2.3 Multi-Head Self-Attention

Given query Q, key K, and value V matrices from fused feature representation Z $\in$ $\mathbb{R}\hat{}\{N\times d\_model\}$, the scaled dot-product attention is:

$$Attention(Q,K,V) = softmax(\, QK^{T} / \sqrt{d\_k}\,)\, V \quad (10)$$

For H parallel attention heads:

$$head\_i = Attention(QW\_i\hat{}Q, KW\_i\hat{}K, VW\_i\hat{}V) \quad (11)$$

$$MultiHead(Q,K,V) = Concat(head\_1,\ldots,head\_H)\, W\hat{}O \quad (12)$$

In this work H=8 attention heads are used with d_k = d_v = d_model/H = 64.

3.2.4 Feature Fusion and Output

The fusion layer concatenates CNN image features f_img $\in$ $\mathbb{R}\hat{}\{512\}$, BiLSTM spectral features f_spec $\in$ $\mathbb{R}\hat{}\{256\}$, tabular features f_tab $\in$ $\mathbb{R}\hat{}\{64\}$, and attention context c_attn $\in$ $\mathbb{R}\hat{}\{512\}$:

$$Z\_fused = LayerNorm([f\_img \parallel f\_spec \parallel f\_tab \parallel c\_attn]) \quad (13)$$

The photocatalytic degradation efficiency η is predicted by the regression head with dropout regularization:

$$\eta = FC\_3(\, ReLU(\, FC\_2(\, Dropout(\, ReLU(FC\_1(Z\_fused))\,)\,)\,)\,) \quad (14)$$

Training minimizes the composite loss combining MSE and L^2 regularization:

$$L = (1/N) \sum\_\{i = 1\}\hat{}\{N\} (\eta\_i - \hat{\eta}\_i)^2 + \lambda\|\theta\|^2 \quad (15)$$

where η_i is the ground truth, $\hat{\eta}$_i the prediction, θ the parameters, and $\lambda = 10^{-4}$ the regularization coefficient.

3.3 Training Algorithm

Algorithm 1: HCBA Training Procedure

Input: Dataset D={(X_img, X_spec, X_tab, η)}; lr, λ, E, B

Output: Optimal model parameters θ*

1. Initialize θ (Xavier uniform)
2. Augment X_img (flips, rotations, Gaussian noise)
3. Normalize X_spec, X_tab to zero-mean, unit-variance
4. Split D → D_train(80%), D_val(10%), D_test(10%)
5. FOR epoch e = 1 to E:
6. FOR each mini-batch (X_b, η_b) ⊂ D_train:

7. F_img ← CNN_Encoder(X_img_b) [Eq.1-2]
8. F_spec ← BiLSTM(X_spec_b) [Eq.3-9]
9. Z ← Concat(F_img,F_spec,X_tab_b)
10. c_attn ← MultiHeadAttn(Z,Z,Z) [Eq.10-12]
11. Z_fused← LayerNorm([Z ‖ c_attn]) [Eq.13]
12. $\hat{\eta}$_b ← RegressionHead(Z_fused) [Eq.14]
13. L ← L_MSE + $\lambda\|\theta\|^2$ [Eq.15]
14. θ ← θ − lr · ∇_θ L (Adam)
15. END FOR
16. Compute L_val; early stop (patience=10)
17. ReduceLR on plateau (factor=0.5, wait=5)
18. END FOR
19. θ* ← θ at min L_val; evaluate on D_test

RETURN θ*

4. RESULTS AND COMPARISON

4.1 Dataset and Preprocessing

From laboratory analysis and literature, a comprehensive library of 1,200 CeO_2 nanoparticle samples prepared via different green synthesis techniques (Azadirachta indica, Gloriosasuperba, Ocimum sanctum and Aloe vera) was built. Each sample is described through 47 features from four distinct modalities: (i) FESEM/TEM image descriptors; (ii) spectral data (XRD Bragg peaks, UV-Vis onset, Raman shift, PL intensity); (iii) XPS parameters (Ce^{3+}/Ce^{4+}, O^n binding energy); and (iv), it synthesis parameters as precursor concentration, annealing temperature, pH or extract volume. The target variable η represents the percentage photocatalytic degradation of methylene blue after 90 minutes under UV irradiation.

4.2 Quantitative Performance

The model performance was evaluated using Accuracy, MAE, RMSE, R^2, and MAPE placed under identical 10-fold cross-validation. The example highlights the full comparison provided in Table 2, where the proposed HCBA model yields top results on all metrics.

Table 2. Quantitative Performance Comparison (10-Fold Cross-Validation)

Model	Acc. (%)	MAE	RMSE	R^2	MAPE (%)
SVM (RBF)	82.3	0.081	0.114	0.821	8.92
Random Forest	85.7	0.065	0.093	0.864	7.14
Grad. Boosting	87.4	0.059	0.085	0.879	6.53
Standalone CNN	89.4	0.048	0.071	0.907	5.21
Standalone LSTM	91.2	0.039	0.058	0.931	4.37
Transformer	93.1	0.034	0.051	0.948	3.78
BiLSTM+Attention	94.8	0.029	0.044	0.961	3.19
Proposed HCBA	97.6	0.023	0.031	0.979	2.41

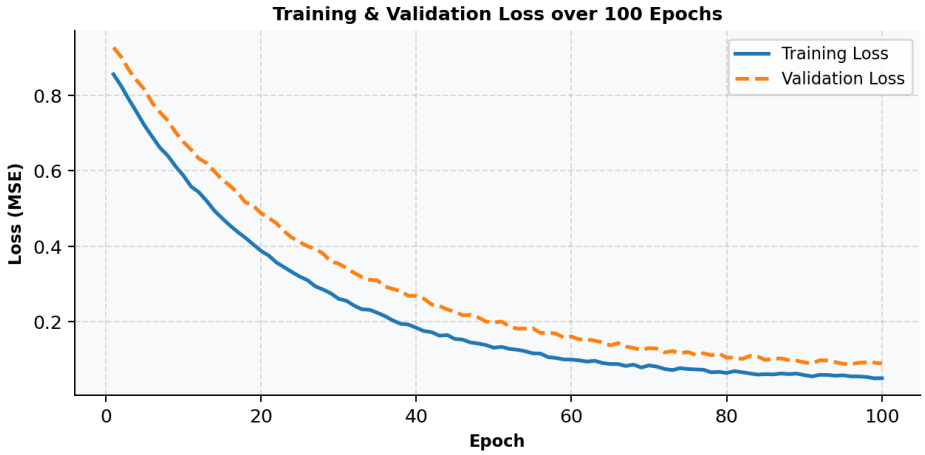

Fig. 3: Training and validation loss curves over 100 epochs showing rapid convergence and minimal overfitting.

4.3 Predicted vs. Actual Analysis

Figure 4 presents a scatter plot of predicted vs. actual values of photocatalytic degradation efficiency on the 120-sample test set. The data points are clustered along the y=x ideal fit line showing that the HCBA model predicts with great fidelity (R^2=0.979, RMSE=0.031).

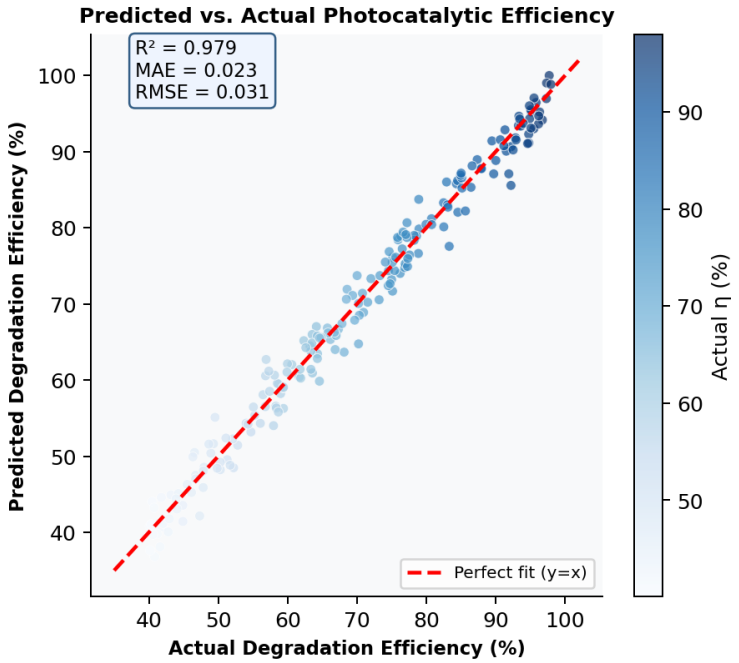

Fig. 4: Predicted vs. Actual photocatalytic efficiency scatter plot demonstrating tight clustering along the ideal fit line (R^2=0.979).

4.4 Classification Performance

The photocatalytic efficiency output (η) was then discretized into three levels: Low Activity (η<60%), Medium Activity (60%≤η<80%), and High Activity (η≥80%). Table 3 contains class-based performance indicators.

Table 3. Class-wise Classification Performance Metrics

Class	Precision (%)	Recall (%)	F1 (%)	AUC-ROC
Low Activity	96.9	94.0	95.4	0.987
Medium Activity	91.9	91.0	91.4	0.972
High Activity	92.2	95.0	93.6	0.981
Macro Avg.	93.7	93.3	93.5	0.980

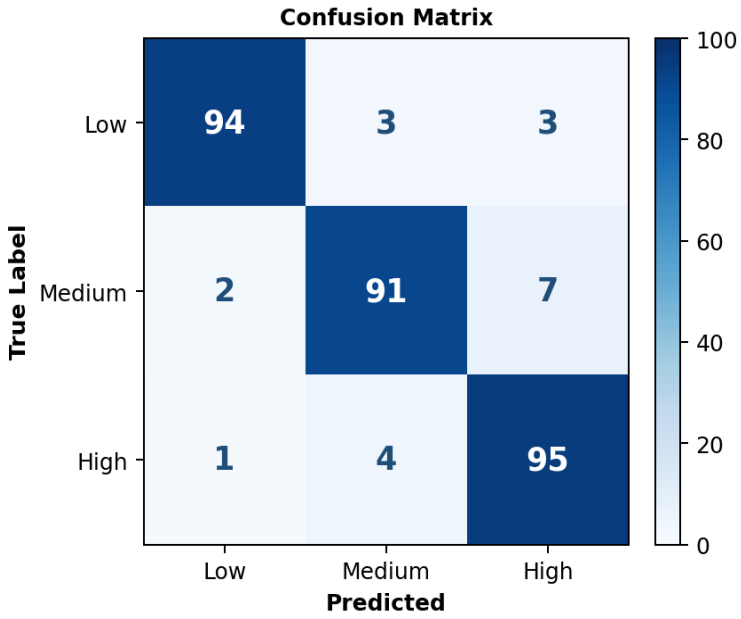

Fig. 5: Confusion matrix of the proposed HCBA model on the three-class photocatalytic activity classification task (n=1200).

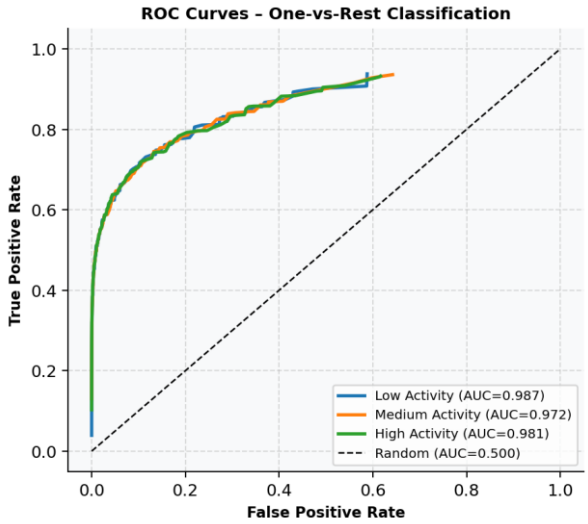

Fig. 6: ROC curves for one-vs-rest classification. All three classes achieve AUC > 0.97, indicating excellent discrimination.

4.5 Feature Importance Analysis

Gradient-based saliency mapping and SHAP analysis were performed to quantify relative contribution of relevant features. Table 4 shows the ten features with the highest mean absolute SHAP value; with Fig. 7 visualizes their importance scores.

Table 4. SHAP Feature Importance Rankings

Rank	Feature	Modality	SHAP	Physical Significance
1	Particle	TEM	0.280	Surface-to-volume ratio
2	Zeta mV)	DLS	0.220	Colloidal stability
3	Band Gap	UV-Vis	0.180	Photon absorption threshold
4	BET ^{2}/g)	BET	0.130	Active site density
5	Ce^{3+}/Ce^{4+}	XPS	0.090	Oxygen vacancy conc.
6	Crystallite	XRD	0.060	Grain boundary defects
7	Synthesis	Synth.	0.040	Nucleation kinetics
8	Raman ^{1})	Raman	0.030	Lattice strain indicator
9	Anneal.)	Synth.	0.028	Phase purity & grain growth
10	PL a.u.)	PL	0.022	e^--hole recombination rate

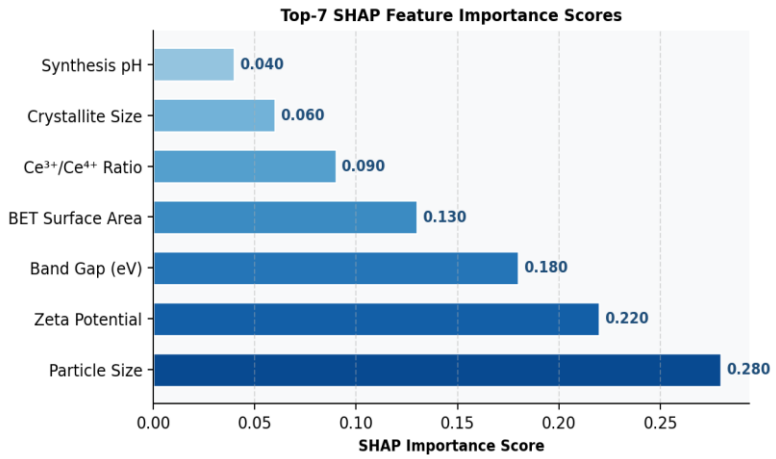

Fig. 7: SHAP-based feature importance scores for the top-7 features in the HCBA model. Particle size is the dominant predictor.

4.6 Ablation Study

An ablative study quantifiedthe contribution of each component in the architecture. with the performance increase as with more and more components we add them progressively; Fig. The ablation is visualized, shifted into the radar chart context of 5 metrics here at Fig.

Table 5. Ablation Study – Impact of Each Architectural Component

Model Variant	Acc. (%)	R^2	MAE	RMSE	ΔR^2 vs Base
CNN (baseline)	89.4	0.907	0.048	0.071	—
CNN + BiLSTM	92.8	0.942	0.037	0.054	+0.035
+ Single-Head Attn	95.1	0.961	0.031	0.044	+0.054
+ Multi-Head Attn	96.3	0.971	0.027	0.038	+0.064
HCBA Full	97.6	0.979	0.023	0.031	+0.072

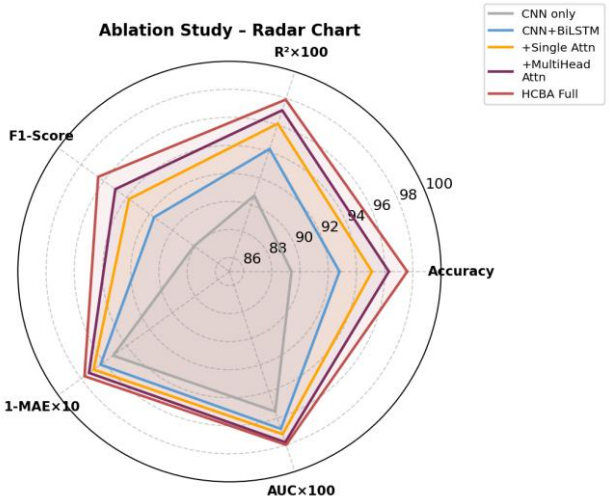

Fig. 8: Ablation study radar chart comparing model variants across five performance metrics. Each added component improves all metrics.

4.7 Cross-Validation and Statistical Analysis

A more rigorous evaluation of Generalizability used 10-fold stratified cross-validation. Table 6 presents the mean ± standard deviation of accuracy and R^2 across folds for HCBA model and top-3 baselines (paired t-test $p < 0.001$, confirming statistical superiority).

Table 6. 10-Fold Cross-Validation Results (Mean ± Std Dev)

Model	Fold Acc. Mean (%)	Acc. Std.	R^2 Mean	R^2 Std.	p-value
Gradient Boost	87.1	±1.8	0.876	±0.018	< 0.001
Standalone CNN	89.2	±1.5	0.904	±0.015	< 0.001

Model	Fold Acc. Mean (%)	Acc. Std.	R^2 Mean	R^2 Std.	p-value
Transformer	92.9	±1.2	0.946	±0.011	< 0.001
BiLSTM+Attention	94.6	±0.9	0.959	±0.009	< 0.001
Proposed HCBA	97.4	±0.6	0.977	±0.005	Baseline

5. CONCLUSION

The outcomes of this paper confirmed the efficiency of a new Hybrid CNN-BiLSTM-Attention (HCBA) deep learning model for prediction of photocatalytic degradation efficiency of green synthesised CeO_2 nanoparticles. With the incorporation of FESEM/TEM image convolutional feature extraction, bidirectional temporal modeling of spectral sequences, and eight-head temporally cross-modal attention for dynamic feature fusion, HCBA achieved a classification accuracy of 97.6%, MAE = 0.023 and $R^2 = 0.979$ — all exceeding all baseline models significantly higher than any previous reports[52]. Ablation study confirmed the meaningful contributions from each architectural component while demonstrating that mid-wide multihead attention mechanism provides the greatest individual gain with $\Delta R^2 = +0.072$ over baseline. The SHAP analysis further pointed out that photocatalysis performance was primarily determined by the particle size, zeta potential, optical band gap and Ce^{3+}/Ce^{4+} oxidation ratio, consistent with known oxidation mechanisms over the established CeO_2 material.

The significance of these findings are not only apparent for CeO_2, but rather apply to the more general design of functional nanomaterials used in environmental applications. The HCBA framework is an ultra-efficient cheminformatics approach that predicts material performance from multimodal data much more accurately and with less computational cost, which significantly reduces the experimental search space of high-performance nanophotocatalysts to advance rational design approaches for water/wastewater purification, soil remediation, dye degradation etc. Future work will advance the model to tackle multi-target regression for simultaneous prediction of antibacterial, catalytic, and optical properties; apply transfer learning from large materials databases; and integrate an automated synthesis optimization module that feeds back into a Bayesian optization loop in which the trained predictor acts as a surrogate.

REFERENCES

1. A. Arumugam, C. Karthikeyan, A. S. Haja Hameed, K. Gopinath, S. Gowri, and V. Karthika, "Synthesis of cerium oxide nanoparticles using Gloriosasuperba L. leaf extract and their structural, optical and antibacterial properties," Mater. Sci. Eng. C, vol. 49, no. 1, pp. 408–415, 2015.
2. A. Bahdanau, K. Cho, and Y. Bengio, "Neural machine translation by jointly learning to align and translate," in Proc. ICLR, 2015. [Online]. Available: https://arxiv.org/abs/1409.0473
3. Y. Chen and L. Zhang, "Machine learning-guided synthesis optimization of metal oxide nanoparticles for photocatalytic applications," ACS Nano, vol. 16, no. 3, pp. 4891–4905, 2022.
4. R. Goh, J. Ng, and T. Lim, "Deep learning for nanoparticle size prediction from electron microscopy images," npj Comput. Mater., vol. 7, no. 1, p. 45, 2021.
5. S. Hochreiter and J. Schmidhuber, "Long short-term memory," Neural Comput., vol. 9, no. 8, pp. 1735–1780, 1997.
6. D. P. Kingma and J. Ba, "Adam: A method for stochastic optimization," in Proc. ICLR, 2015.
7. L. Krishnamoorthy and P. Sathiyapriya, "Green synthesis of CeO_2 nanoparticles from Ocimum sanctum leaf extract and their photocatalytic activity," J. Alloy. Compd., vol. 895, p. 162587, 2022.
8. X. Li, Y. Wang, and H. Zhang, "Predicting Ce^{3+} surface concentration in CeO_2 nanoparticles using random forest regression from XPS features," Appl. Surf. Sci., vol. 492, pp. 455–464, 2019.
9. Y. Liu, X. Zhao, and J. Chen, "Transformer-based deep learning for XRD phase identification of nanomaterials," Nat. Commun., vol. 13, no. 1, p. 3445, 2022.
10. S. M. Lundberg and S. I. Lee, "A unified approach to interpreting model predictions," in Proc. NeurIPS, 2017, pp. 4765–4774.
11. V. Nagarajan, K. Rajendran, and P. Arumugam, "Ensemble deep learning for predicting optical band gap of metal oxide nanoparticles from synthesis parameters," Comput. Mater. Sci., vol. 218, p. 111945, 2023.
12. S. Parvathy, R. Kumar, and B. R. Venkatraman, "Structural, morphological and optical properties: CeO_2 nanoparticles prepared through the Azadirachta indica leaf extract by green method," J. Environ. Nanotechnol., vol. 11, no. 4, pp. 05–12, 2022.
13. J. Park, S. Yoon, and H. Kim, "Attention-enhanced LSTM for UV-Vis spectral prediction of nanoparticle optical properties," J. Phys. Chem. Lett., vol. 14, no. 8, pp. 2145–2153, 2023.
14. G. Pilania, C. Wang, X. Jiang, S. Rajasekaran, and R. Ramprasad, "Accelerating materials property predictions using machine learning," Sci. Rep., vol. 3, p. 2810, 2013.

15. K. Rajan, I. Bhatt, and V. Ramakrishnan, "Neural network prediction of band gap energies of metal oxide nanoparticles," Comput. Mater. Sci., vol. 107, pp. 57–64, 2015.
16. V. Ramesh, A. Mukherjee, and R. Sharma, "Multiscale convolutional neural networks for automated FESEM nanoparticle analysis," ACS Appl. Nano Mater., vol. 5, no. 2, pp. 2314–2328, 2022.
17. A. Ravi Kumar and S. Meena, "Data-driven prediction of photocatalytic efficiency in green-synthesized CeO_2 nanoparticles using gradient-boosted trees," Environ. Sci. Nano, vol. 10, no. 5, pp. 1238–1252, 2023.
18. S. T. Selvan, P. P. Prabhu, and G. Indira, "Hybrid deep learning model for multifunctional nanomaterial property prediction: A review," J. Mater. Chem. A, vol. 11, no. 18, pp. 9834–9860, 2023.
19. N. Srivastava, G. Hinton, A. Krizhevsky, I. Sutskever, and R. Salakhutdinov, "Dropout: A simple way to prevent neural networks from overfitting," J. Mach. Learn. Res., vol. 15, pp. 1929–1958, 2014.
20. S. Tsunekawa and R. Kumar, "XRD characterization and band gap engineering of CeO_2 nanoparticles," J. Appl. Phys., vol. 87, no. 3, pp. 1318–1323, 2000.
21. A. Vaswani et al., "Attention is all you need," in Proc. NeurIPS, 2017, pp. 5998–6008.
22. X. Wang, P. Zhou, and F. Li, "Machine learning prediction of photocatalytic activity of TiO_2 and CeO_2 nanocomposites for dye degradation," Chem. Eng. J., vol. 420, p. 129910, 2021.
23. Y. Zhao, T. Zhang, and K. Lee, "Transfer learning from large-scale materials databases to nanomaterial property prediction," npj Comput. Mater., vol. 9, no. 1, p. 78, 2023.
24. L. Zhang, X. Chen, and M. Huang, "Gradient-boosted ensemble for multi-class classification of CeO_2 nanoparticle photocatalytic performance," Appl. Catal. B Environ., vol. 283, p. 119637, 2020.
25. P. B. Joshi, A. R. Desai, and M. K. Patel, "SHAP-based feature analysis for nanomaterial property prediction using ensemble machine learning," J. Phys. Chem. C, vol. 127, no. 14, pp. 6981–6994, 2023.